Biosensors and Bioelectronics 142 (2019) 111569

Contents lists available at ScienceDirect

Biosensors and Bioelectronics

journal homepage: www.elsevier.com/locate/bios

Coupling photoelectrochemical and electrochemical strategies in one probe electrode: Toward sensitive and reliable dual-signal bioassay for uracil-DNA glycosylase activity

Yanwei Lu, Huan Zhao, Gao-Chao Fan**, Xiliang Luo*

Key Laboratory of Optic-electric Sensing and Analytical Chemistry for Life Science, MOE, Shandong Key Laboratory of Biochemical Analysis, College of Chemistry and Molecular Engineering, Qingdao University of Science and Technology, Qingdao, 266042, China

ARTICLE INFO

Keywords:
Uracil-DNA glycosylase
Photoelectrochemistry
Electrochemistry
Dual-signal bioassay

ABSTRACT

Uracil-DNA glycosylase (UDG) is a typical initiator for base excision repair (BER) process. Since aberrant expression of UDG is relevant to a variety of cancers, analysis of UDG activity with high sensitivity and accuracy is of great importance. We reported herein a sensitive and reliable dual-signal bioassay for UDG activity by coupling photoelectrochemical (PEC) and electrochemical (EC) strategies in one probe electrode. The Au/TiO_2 hybrid was used as a matrix to immobilize substrate DNA (sDNA), which modified with $AgInS_2$ quantum dot (AIS QD) on the terminal. When UDG exist, the base of uracil was eliminated from the sDNA, and the produced apyrimidinic (AP) site could be cleaved by endonuclease IV (Endo. IV) immediately. Under this situation, the PEC labels of AIS QDs were detached from the electrode, resulting in a "signal-off" trend for PEC signal. After assistant DNA (aDNA) was then assembled, the hybridization chain reaction (HCR) was triggered, and EC labels of ferrocene molecules were introduced, producing a "signal-on" trend for EC signal. Besides, as the produced long double-stranded DNA by the HCR had evident steric hindrance, the PEC signal further decreased. Based on this meticulous design, the dual-signal bioassay for UDG activity showed low detection limits of 4.3×10^{-5} and 1.9×10^{-4} U/mL with PEC and EC detection, and accurate analysis of UDG activity in living cells was realized. By just changing the recognition site, this sensitive and reliable dual-signal strategy can be extended to diagnose other DNA repair-related enzymes in the real samples.

1. Introduction

Maintaining genome integrity is the precondition for all organisms to complete gene transcription [Burrell et al., 2013; Hoeijmakers, 2001]. Yet, the structural stability of DNA molecules might be disrupted by various endogenous or exogenous factors, causing genomic instability and inducing various canceration [Forment et al., 2012; Lord and Ashworth, 2012]. Base excision repair (BER) is an important principal mechanism in human body for maintaining genomic integrity by removing damaged DNA bases [Hegde et al., 2008; Ledoux and Wilson, 2004; Maynard et al., 2009]. As a well-known promoter in human body BER process, uracil-DNA glucoamylase (UDG) can recognize specifically and catalyze the hydrolytic cleavage of non-glycosyl bonds between uracil and pentose, leaving an apyrimidinic (AP) site in the uracil-containing DNA [David and Williams, 2002; Duncan and Miller, 1980; Savva et al., 1995; Werner and Stivers, 2000]. Some previous reports confirmed that abnormal activity of UDG could interfere with the normal proceeding of the uracil-included DNA base excision repair process, leading to various disorders such as cancer, Bloom's syndrome, lymphoma, human immunodeficiency and neurodegenerative diseases [Du et al., 2018; Gupta and Sirover, 2006; Imai et al., 2003; Sousa et al., 2007; Wang et al., 2017]. Hence, as a disease marker, accurate and efficient detection of UDG activity is particularly important in the field of biomedicine.

For the detection of UDG activity, a combination method of gel electrophoresis and radiolabeling was initially developed [Boorstein et al., 2001; Sud'ina et al., 2000]. However, this method has some inadequacies such as radiation hazard, low sensitivity, complicated operation and long detection time. In recent years, newly developed techniques for measuring UDG activity include colorimetry [Liu et al., 2014; Nie et al., 2015], electrochemistry [Jiao et al., 2016; Liu et al., 2013], chemiluminescence [Dong et al., 2017; Leung et al., 2013],

* Corresponding author.
** Corresponding author.
E-mail addresses: gcfan@qust.edu.cn (G.-C. Fan), xiliangluo@qust.edu.cn (X. Luo).

https://doi.org/10.1016/j.bios.2019.111569
Received 13 June 2019; Received in revised form 23 July 2019; Accepted 2 August 2019
Available online 02 August 2019

fluorescence [Lee et al., 2015; Wu et al., 2015], and the like. In the methods above, a substrate DNA containing a plurality of uracil bases is generally used as an identification site of UDG. However, when the UDG concentration is extremely low, especially for biological samples that are usually in a cell or serum environment, the UDG activity cannot cause sufficient signal changes for the purpose of detection. Meanwhile, since the detection signal of the conventional detection method is just a single signal output model, some factors such as ambient environment or complicated operations could unavoidably influence the signal output. Dual signal output sensors contain intrinsic corrections to the influence of systematic error or background signals [Jiang et al., 2018; Mars et al., 2018; Xu et al., 2016], demonstrating significant potential for further improved accuracy and sensitivity in practical applications. Therefore, it is very desirable to find an accurate and reliable dual-signal analysis with two different transduction mechanisms.

Electrochemical (EC) technique has attracted wide attention from researchers because of their low cost, fast operation speed, small size and good stability [Hu et al., 2018; Saidur et al., 2017; Song et al., 2016; Ricci et al., 2012]. Photoelectrochemical (PEC) technique is a new generation of electrochemical method, which recently has shown its promising potential in various bioanalysis because of its exciting features of simple device, low background signal, and potential high sensitivity [Wang et al., 2015; Fan et al., 2016; Li et al., 2018; Qiu et al., 2019]. Herein, we first developed a dual-signal bioassay integrating PEC with EC strategies in one probe electrode for sensitive and accurate detection of UDG activity, as outlined in Scheme 1. Specifically, TiO_2 and Au nanoparticles were first modified sequentially on a clean indium–tin oxide (ITO) electrode to form an Au/TiO_2 matrix for immobilizing substrate DNA (sDNA) and blocking reagent of 6-mercapto-1-hexanol (MCH). $AgInS_2$ quantum dots (AIS QDs) as PEC labels were bound covalently on the sDNA, producing sensitization structure between the AIS QDs and the Au/TiO_2 matrix. In the existence of UDG, the uracil in sDNA would be removed, and meanwhile, the produced apyrimidinic (AP) site could be cleaved by endonuclease IV (Endo. IV) to release the PEC labels of AIS QDs from the electrode surface. In this case, the PEC signal of the probe electrode decreased owning to disappeared sensitization effect of the AIS QDs to the Au/TiO_2 matrix. After assistant DNA (aDNA) was then assembled on the electrode, abundant EC labels of ferrocene molecules were introduced on the electrode via the hybridization chain reaction (HCR) process, producing an evident increased EC signal. Besides, as the long double-stranded DNA produced by the HCR process has obvious steric hindrance to inhibit photogenerated electron transfer, the PEC signal further decreased. Thus, a sensitive, accurate and reliable dual-signal bioassay with "signal-off" PEC and "signal-on" EC strategies for UDG activity was realized.

2. Experimental

2.1. Materials and reagents

Indium tin oxide (ITO) glass was obtained from Zhuhai Kaivo Optoelectronic Technology Co., Ltd. (China). TiO_2 powder (P25), triethanolamine, thioacetamide and silver nitrate were purchased from Alfa Aesar (China). 3-Mercaptopropionic acid (MPA), indium (III) nitrate hydrate, N-hydroxysuccinimide (NHS), silver (I) nitrate ($AgNO_3$), and 3-(3-dimethylaminopropyl)-1-ethylcarbodiimide hydrochloride (EDC) were purchased from Sigma-Aldrich Inc. (USA). Sodium sulfide nonahydrate ($Na_2S{\cdot}9H_2O$), chloroauric acid ($HAuCl_4$), ascorbic acid (AA), and potassium chloride (KCl) was purchased from Sinopharm Chemical Reagent Co., Ltd. (China). All other reagents involved were of analytical grade. All aqueous solutions were prepared with deionized water (DI water, 18 MΩ/cm), which was obtained from a Milli-Q water purification system. The BCA protein assay kit, uracil-DNA glycosylase (UDG) and endonuclease IV (Endo. IV) were purchased from Sangon Inc. (Shanghai, China). The UDG inhibitor (UGI) was obtained from New England Biolabs (Beijing, China).

All DNA oligonucleotides were synthesized by Sangon Inc. (Shanghai, China) with the sequences as follows:

Substrate DNA (sDNA): 5′-NH_2-TTT TTT UTT TTC ACU AAC ACG GAG TGA AAA AAA AAA ATT TTT T-SH-3';

Assistant DNA (aDNA): 5′-ferrocene-TTC ACT CCG TGT TTG AGG TAG TAG GTT GTA TAG TT-3';

H1 DNA: 5′-AGT AGG TTG TAT AGT TCA AAG TAA CTA TAC AAC CTA CTA CCT CA-ferrocene-3';

H2 DNA: 5′-ferrocene-ACT TTG AAC TAT ACA ACC TAC TTG AGG

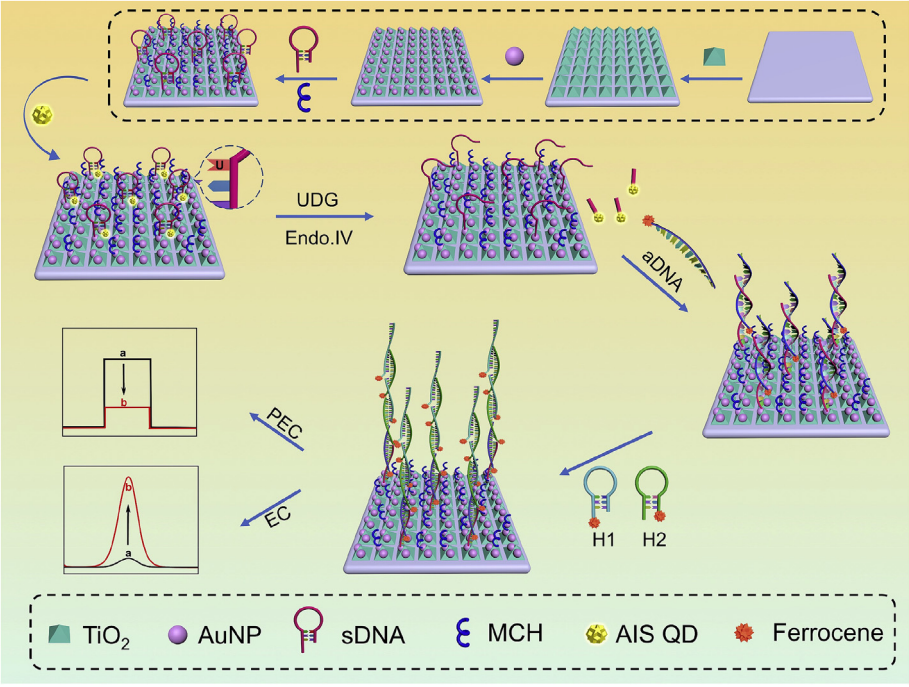

Scheme 1. Development of dual-signal bioassay for UDG activity coupling PEC and EC strategies in one probe electrode.

TAG TAG GTT GTA TAG TT-3'.

2.2. Apparatus

Both PEC and EC measurements were performed on a Zahner PEC workstation (ZAHNER-elektrik GmbH & Co. KG, Germany) with a conventional three-electrode system: a platinum wire as counter electrode, a saturated Ag/AgCl electrode as reference electrode, and a modified Au/TiO_2/ITO matrix with an area of 0.5 × 0.5 cm^2 as working electrode. Scanning electron microscopy (SEM) was carried out on a Hitachi S-4800 scanning electron microscope (Hitachi Co., Japan). Transmission electron microscopy (TEM) was performed by a JEM-2100 transmission electron microscope with an accelerating voltage of 200 kV (Hitach, Japan). Fourier transform infrared (FT-IR) spectroscopy was carried out with a Nicolet iS10 FT-IR spectrometer (Thermo Fisher Scientific, US). UV–visible (UV–vis) absorption spectra were tested on a UV-3600 UV–visible spectrophotometer (Shimadzu, Japan). X-ray photoelectron spectroscopy (XPS) was performed using an ESCALAB 250Xi spectrometer (Thermo Fisher Scientific, UK) with a monochromatic Al Kα X-ray source, and all spectra were calibrated by normalizing the C (1s) peak to the standard value of 284.6 eV. Powder X-ray diffraction (XRD) pattern was obtained from a Philips X'pert Pro X-ray diffractometer (Cu Kα radiation, λ = 0.15418 nm, Netherlands). Electrochemical impedance spectroscopy (EIS) was performed on an Autolab potentiostat/galvanostat (PGSTAT 30, Eco Chemie B.V., Utrecht, Netherlands) with a three-electrode system in 0.1 M KCl containing 5.0 mM $K_3[Fe(CN)_6]/K_4[Fe(CN)_6]$ (1:1) mixture as a redox probe, and recorded in the frequency range of 0.01 Hz–100 kHz with an amplitude of 50 mV.

2.3. Synthesis of AIS QDs

The $AgInS_2$ quantum dots (AIS QDs) were synthesized according to previous paper [Regulacio et al., 2013]. Normally, a 50 mL of the aqueous solution containing 0.1 mmol $AgNO_3$, 0.4 mmol $In(NO_3)_3$ and 0.1 mmol MPA was prepared in a 100 mL three-necked flask. Under vigorous stirring, 3 mL of 0.2 M Na_2S (0.6 mmol) solution was rapidly transfused in the flask. Then, the mixed solution was heated to 100 °C for 2 h to allow the growth of AIS QDs.

2.4. Preparation of Au/TiO_2/ITO matrix

Before preparation, ITO glass was cut into small pieces (2 × 0.5 cm) and ultrasonically treated in order with acetone, 1 M sodium hydroxide water/ethanol mixture (1:1, v/v) and deionized water for 10 min. A quantity of TiO_2 powder was dispersed in DI water by ultrasonic shaking, and then 20 μL of uniformly suspended droplets was added dropwise onto the conductive surface of ITO glass with a modified area of 0.25 cm^2. After the droplets are dried in the air, a uniform film was formed on the ITO glass, which was heated to 450 °C, calcined in an air atmosphere for 30 min, and finally cooled to room temperature, and the obtained electrode was termed as the TiO_2/ITO electrode. By varying the concentrations of TiO_2 suspension, the thicknesses of TiO_2 film could be controlled.

The deposition of Au nanoparticles on the TiO_2/ITO electrode was based on a previous report with some modifications [Xiang et al., 2017]. As a working electrode, the TiO_2/ITO electrode was put into the electrodeposition solution (5 mM $HAuCl_4$ and 0.5 M KCl solution) with an inserted area of 0.25 cm^2. A platinum wire was served as counter electrode, and a saturated Ag/AgCl electrode was used as reference electrode, using constant potential at −0.4 V for 60 s to produce the AuNPs-plated TiO_2/ITO. The resulting Au/TiO_2/ITO matrix was washed with DI water and dried with N_2.

2.5. Development of dual-signal bioassay

Firstly, the sDNA was placed in a 95 °C water bath for 5 min, and then removed to allow it cool to room temperature slowly to form a hairpin structure. Typically, 20 μL of 1.5 μM sDNA was dropped on the Au/TiO_2/ITO matrix and incubated at 4 °C for 12 h. After rinsed with Tris−HCl buffer (10 mM, pH7.4) to remove the unbound sDNA, the electrode was covered with 20 μL of 1 mM MCH for 30 min to block the non-specific binding sites. Subsequently, the electrode was immerged into an $AgInS_2$ QDs solution containing 10 mM EDC/NHS for 1 h and then rinsed with Tris-HCl buffer. Next, 20 μL of excision reaction buffer (containing different concentrations of UDG, 0.5 U of Endo. IV, and 2 μL of 10 × UDG reaction buffer) was dropped on the surface of the modified electrode to incubate at 37 °C for 60 min. After the treatment of UDG and Endo. IV, 20 μL of 1 μM aDNA (labeled with ferrocene molecule) was added onto the electrode surface and incubated for 60 min at room temperature. For the hybridization chain reaction (HCR) process, 20 μL of mixture solution containing 1 μM H1 DNA and 1 μM H2 DNA, both of which were labeled with ferrocene molecules, was scattered onto the electrode surface and further incubated for 2 h at room temperature. After rinsed with Tris-HCl buffer, the electrode was finally ready for PEC and EC measurements.

For preliminary application of the dual-signal bioassay in living cells, cancer cells of HeLa, HepG2 and MCF-7 were selected as the model targets. And the detail for cell culture and sample preparation was presented in the Supporting information.

2.6. PEC and EC measurements

Chopped light voltammetry was employed for PEC detection with the applied voltage of 0.0 V, which was implemented at room temperature in phosphate buffer solution (PBS, pH 7.4, 0.1 M) containing 0.1 M ascorbic acid (AA). A light-emitting-diode (LED) lamp with light intensity of 350 W/m^2 and an emission wavelength of 430 nm was utilized as irradiation source, which was switched on and off every 10 s.

Square wave voltammetry (SWV) was employed for EC detection with a 25 mV amplitude signal, a range from 0.1 V to 0.7 V versus Ag/AgCl reference, a step potential of 4 mV and a frequency of 10 Hz, which was carried out at room temperature in PBS (pH 7.4, 0.1 M).

3. Results and discussion

3.1. Characterization of AIS QDs

Fig. 1A shows TEM image of the AIS QDs, from which many spherical QDs could be observed. The inset of Fig. 1A reveals high-resolution TEM image of the AIS QDs, and an average diameter of 4.0 nm was obtained from the clear lattice fringes and outline of the QDs. Fig. 1B displays UV–vis absorption spectrum of the AIS QDs, which exhibited a broad absorption range below 553 nm. The absorption of AIS QDs lacks an obvious excitonic peak deriving from defect sites within the bandgap. The inset in Fig. 1B presents photographs of the obtained AIS QDs aqueous solution under white light and UV-lamp, respectively. The high brightness orangefl-uorescence illustrated high quality of the AIS QDs. Fig. 1C displays FT-IR spectrum of the AIS QDs. The strong peak at 3400 cm^{-1} and 1680 cm^{-1} are in accordance with the hydroxide group and carbonyl group, which indicated that the surface of the AIS QDs were modified with carboxyl groups coming from MPA molecules. The XRD pattern of the as-obtained AIS QDs is shown in Fig. 1D, in which the four unambiguous dffiraction peaks at 2θ = 27.2°, 45.1°, 50.5° and 60.1° could be assigned to the (112), (204), (312) and (400) planes of tetragonal $AgInS_2$ (JCPDS No. 25–1330). Based on the standard XRD patterns of Ag_2S (JCPDS No. 04–0774) and In_2S_3 (JCPDS No. 33–0623), the XRD pattern did not appear these impurities' diffraction peaks, illustrating high purity of the synthesized AIS QDs.

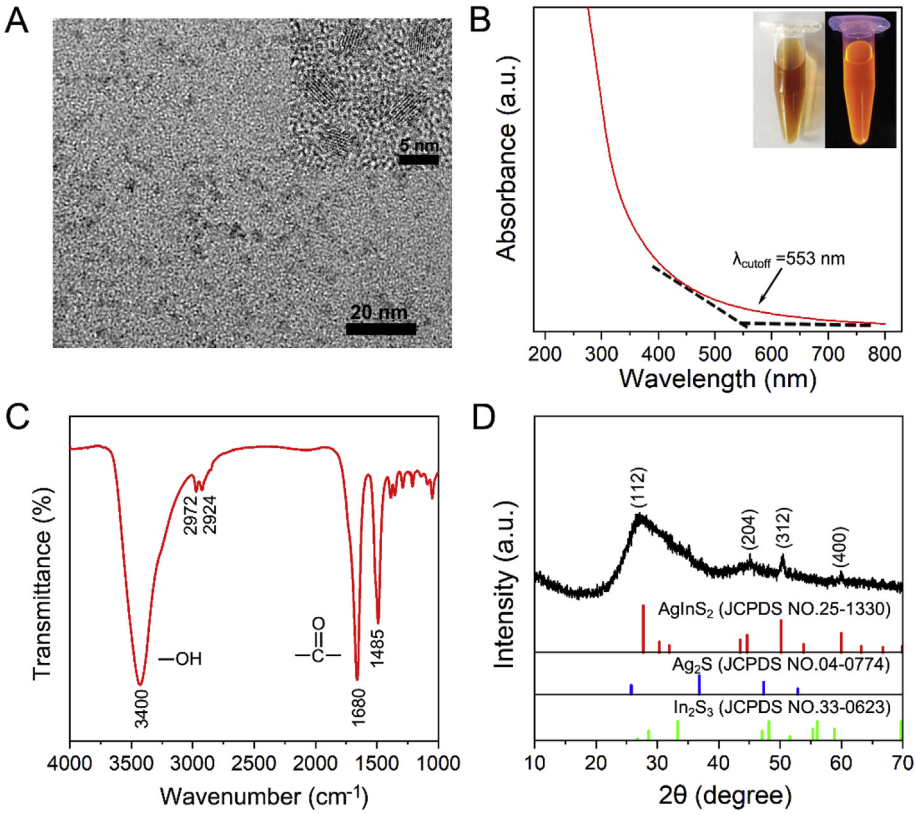

Fig. 1. TEM image, UV–vis absorption spectrum, FT-IR spectrum and XRD pattern of the synthesized AIS QDs (A to D). Insets in B: photographs of AIS QDs solution under white light and UV-lamp.

3.2. Characterization of Au/TiO_2/ITO matrix

Fig. 2A and B displays typical SEM images of the TiO_2/ITO and Au/TiO_2/ITO electrodes, respectively. It could be observed that plenty of TiO_2 nanoparticles with grain size range of 20–30 nm were covered onto the ITO surface and formed a mesoporous film (Fig. 2A). After deposition produce of Au, it can be clearly seen that many smaller particles with the average size of 10–15 nm were decorated on the TiO_2 film (Fig. 2B). Besides, the elemental mapping analysis in the insets of Fig. 2A and B also illustrated the deposition of Au nanoparticles on the TiO_2/ITO electrode and the decorated Au element was homogeneously distributed on the TiO_2 film. The results thus verified the successful formation of the Au/TiO_2/ITO matrix. XPS was further used to determine chemical composition and valence states of the Au/TiO_2/ITO matrix, as shown in Fig. 2C. The spectrum of the TiO_2/ITO electrode shows XPS peaks of Ti 3p, C 1s, In 3d, Ti 2p, O 1s, and Ti 2s peaks (black curve). Among these XPS peaks, Ti 3p, Ti 2p, O 1s and Ti 2p were from TiO_2, while C 1s was used as the internal reference to calibrate the binding energy and In 3d was from the ITO substrate. After deposition produce of Au, the additional XPS peak of Au 4f appeared (red curve), indicating the modification of Au on the surface of TiO_2/ITO electrode. Thus, XPS characterization further proved successful preparation of the Au/TiO_2/ITO matrix.

3.3. Sensitization effect of AIS QDs to Au/TiO_2 matrix

The schematic diagram to PEC process of the AIS/Au/TiO_2 sensitization structure was illustrated in Fig. 2D. TiO_2 is an n-type, wide bandgap (~3.2 eV) semiconductor material, which can absorb only the ultraviolet light. However, it possesses the obvious merits of high stability, photoelectric activity, biocompatibility and low cost, making it very suitable for serving as a PEC matrix. $AgInS_2$ (AIS), an important ternary chalcogenide, is an n-type semiconductor with a narrow direct energy-gap (1.87–2.2 eV) and it has some distinct advantages such as low toxicity, high extinction coefficient and excellent optical performance [Guan et al., 2018; Li et al., 2013]. The valence-band (CB) energy (E_{VB}) and conduction-band (CB) energy (E_{CB}) of the synthesized AIS QDs were calculated to be −5.19 eV and −2.95 eV, respectively (See Fig. S1 and its description). According to the previous report [Ameta et al., 2015], the E_{VB} and E_{CB} energy levels of TiO_2 were −7.5 eV and −4.3 eV, respectively. Thus, coupling of AIS with TiO_2 emerged a stepwise energy level arrangement, which could effectively utilize the light energy of visible region, promote the charge transfer and inhibit the electron-hole recombination. Thus, the AIS QDs as PEC labels could evidently enhance the photocurrent response (PEC signal). In addition, the role of the deposited Au nanoparticles herein were mainly to firmly bind with the sDNA via Au–S bond. Incidentally, they could also serve as light-scattering centers to increase light absorption of the AIS QDs and further improve the sensitization effect [Fan et al., 2016; Zarazúa et al., 2010].

3.4. Characterization of dual-signal bioassay

To illustrate successful development of the dual-signal bioassay, the characterizations of PEC, EIS, EC and gel electrophoresis were conducted. Fig. 3A shows PEC signals of the dual-signal bioassay during its development. The Au/TiO_2/ITO matrix had a relatively obvious PEC signal (curve a). After sDNA immobilization and MCH blocking, the PEC signal decreased moderately (curve b), being ascribed to their relatively weak electron transfer ability. After AIS QDs were labeled on the terminal of sDNA, an evidently enhanced PEC signal was obtained (curve c), owning to sensitization effect of the AIS QDs to the Au/TiO_2 matrix. After incubated with UDG and Endo. IV, the PEC signal reduced significantly (curve d), because of the destroyed sensitization effect of the AIS QDs caused by specific recognition and cleavage action of UDG and Endo. IV. After aDNA hybridization and HCR process, the PEC

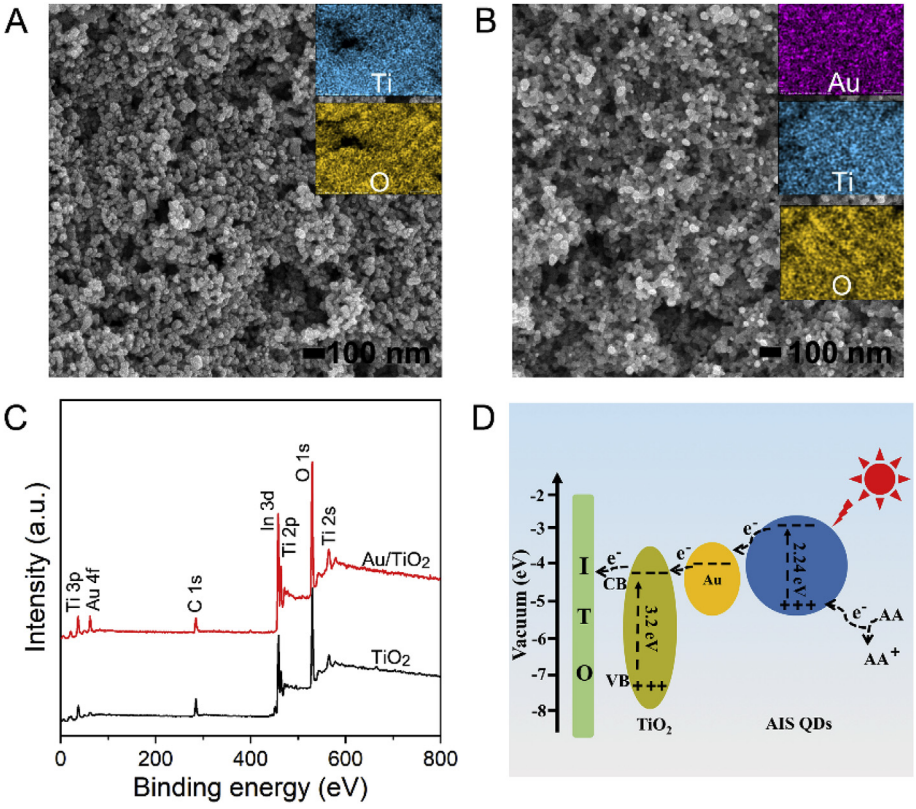

Fig. 2. SEM images of the (A) TiO_2/ITO and (B) Au/TiO_2/ITO electrodes; (C) XPS spectra of the TiO_2 and Au/TiO_2 hybrid; (D) schematic diagram for PEC process of the AIS/Au/TiO_2 sensitization structure. Insets in A and B: elemental mapping analysis of (Ti and O) and (Ti, O and Au), respectively.

signal further decreased (curve e), resulting from evident steric hindrance of the produced long double-stranded DNA by the HCR process.

Fig. 3B shows electrochemical impedance spectra (EIS) of the dual-signal bioassay development. The electron-transfer resistance (R_{et}) was expressed by semicircle diameter of the curve. The Au/TiO_2/ITO matrix had a very small R_{et} (curve a), owning to excellent electrical conductivity of the deposited Au. After sDNA immobilization and MCH blocking, the R_{et} increased (curve b), which was result from their

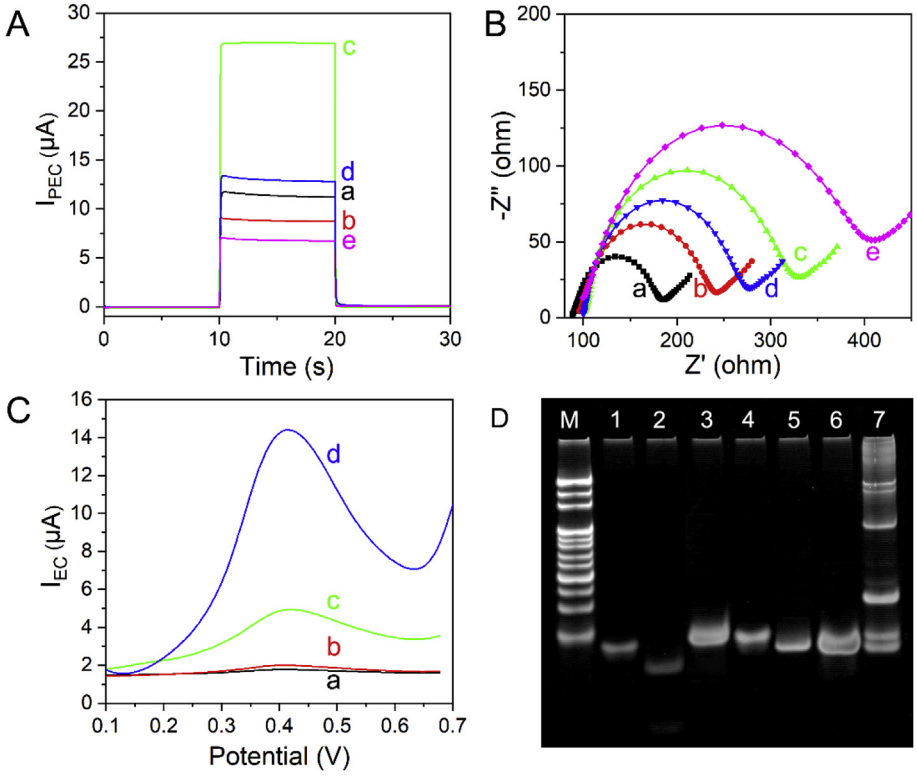

Fig. 3. (A) PEC signals and (B) EIS of (a) the Au/TiO_2/ITO matrix, (b) after sDNA immobilization and MCH blocking, (c) after AIS QDs labeling, (d) after UDG and Endo. IV incubation, and (e) after aDNA hybridization and HCR process. (C) EC signals of (a) the AIS/MCH/sDNA/Au/TiO_2/ITO electrode, (b) after UDG and Endo. IV incubation, (c) after aDNA hybridization, and (d) after HCR process. (D) Native PAGE images of different samples. Lane M: DNA ladder marker; Lane 1: sDNA; Lane 2: UDG and Endo. IV treatment of sDNA; Lane 3: aDNA; Lane 4: H1 DNA; Lane 5: H2 DNA; Lane 6: H1 DNA and H2 DNA; Lane 7: aDNA, H1 DNA and H2 DNA.

relatively low conductivity. After labeled AIS QDs on the terminal of sDNA, the R_{et} further increased (curve c), owning to low conductivity of the semiconductor materials. After incubated with UDG and Endo. IV, the R_{et} decreased evidently (curve d), because of the detached short DNA fragments labeling with AIS QDs caused by specific recognition and cleavage action of UDG and Endo. IV. After aDNA hybridization and HCR process, the R_{et} increased dramatically (curve e), owning to evident steric hindrance and low conductivity of the produced long double-stranded DNA.

Fig. 3C shows EC signals of the dual-signal bioassay during its development. Before aDNA hybridization, the modified electrodes shows ignored EC signals (curves a and b), because no EC labels of ferrocene molecules were introduced. After aDNA hybridization, a moderate EC signal at about 0.4 V was observed (curve c), due to the labeling of ferrocene molecules on the terminal of aDNA. After HCR process, the EC signal at about 0.4 V enhanced significantly, thanks to the labeling of ferrocene molecules on the terminal of both H1 DNA and H2 DNA for hybridization chain reaction.

For the purpose of further verifying the development of the dual-signal bioassay, the UDG activity and HCR amplification reaction were conducted by gel electrophoresis, as shown in Fig. 3D. The lane 1 was corresponding to the sDNA. When UDG and Endo. IV treatment, the hairpin structure of sDNA was destroyed and divided into two fragments (the lane 2). The lanes 3, 4 and 5 were in order corresponding to the single aDNA, H1 DNA and H2 DNA. The lane 6 did not show many bright bands, indicating that the mixture of H1 DNA and H2 DNA could not trigger the HCR amplification. In contrast, the lane 7 displayed many bright bands, confirming that the mixture of the aDNA, H1 DNA and H2 DNA triggered the HCR amplification reaction. Hence, all these results above from the characterizations of PEC, EIS, EC and gel electrophoresis jointly demonstrated the successful construction of the dual-signal bioassay.

3.5. Detection performance of dual-signal bioassay

Under optimal experimental conditions (see Fig. S2 and its description), the detection performance of the dual-signal bioassay was investigated by observing and analyzing the PEC and EC signals with the change of UDG concentration. As shown in Fig. 4A, the PEC signal gradually weakened with the increase in the concentration of UDG, which was derived from gradual decrease of sensitization effect of the PEC labels (AIS QDs) coupled with gradual increase of steric hindrance of the produced long double-stranded DNA by the HCR. Fig. 4B shows the corresponding linear relationship between PEC signal and the logarithm of the concentration of UDG from 1.0×10^{-4} to 0.1 U/mL. The regression equation was $-\Delta I_{PEC} = 26.28 + 5.87\ lgC_{UDG}$ (U/mL) with a correlation coefficient (R^2) of 0.992, and the detection limit was calculated to be 4.3×10^{-5} U/mL (S/N = 3). At the same time, with the increase in the UDG concentration, the EC signal gradually enhanced, as shown in Fig. 4C, which was attributed to evident increase of the EC labels (ferrocene molecules) on the electrode by the HCR. Fig. 4D reveals the corresponding linear relationship between EC signal and the logarithm of the concentration of UDG from 5.0×10^{-4} to 0.1 U/mL. The regression equation was $\Delta I_{EC} = 17.64 + 3.97\ lgC_{UDG}$ (U/mL) with a correlation coefficient (R^2) of 0.989, and the detection limit was calculated to be 1.9×10^{-4} U/mL (S/N = 3). It could be observed that the well-elaborated dual-signal bioassay exhibited higher or comparable analytical performance than most of the related reports [Du et al., 2017, 2018; Leung et al., 2013; Liu et al., 2013; Nie et al., 2015; Wang et al., 2017].

3.6. Selectivity, reproducibility and stability evolution

The selectivity of the developed dual-signal bioassay was assessed by using different kinds of interfering species including human 8-oxoguanine-DNA glycosylase 1 (hOGG1), human alkyl adenine DNA glycosylase (hAAG), human serum albumin (HSA), and telomerase (TE). As shown in Fig. 5A, under identical experimental conditions, obvious signal responses for both ΔI_{EC} and $|\Delta I_{PEC}|$ could be found in the presence of UDG, while no significant signal responses for both ΔI_{EC} and $|\Delta I_{PEC}|$ was found in the presence of hOGG1, hAAG, BSA and TE, demonstrating that the dual-signal bioassay had excellent selectivity for UDG activity detection.

The repeatability of the designed dual-signal bioassay was evaluated by analyzing five independently prepared probe electrodes, as shown in Fig. S3. The relative standard deviations (RSDs) against the PEC (EC) detection of UDG activity at the concentrations of 1.0×10^{-3}, 5.0×10^{-3} and 1.0×10^{-2} U/mL were 3.2% (4.2%), 3.9% (3.5%), and 4.5% (3.1%), respectively. These results reflected a favorable reproducibility of the dual-signal bioassay.

The stability of the developed dual-signal bioassay was inspected by recording the PEC and EC signals of five independently prepared probe electrodes every other day, as shown in Fig. S4. After one week, the PEC and EC signal values obtained were about 92.1% and 94.3% of the original value on the first day, indicating good storage stability of the dual-signal bioassay for UDG activity detection.

3.7. Preliminary application of dual-signal bioassay

Accurate and efficient detection of UDG activity in living cells is particularly critical in the field of biomedicine. Herein, HeLa, MCF-7, and HepG2 cancer cells were selected as the model targets to verify potential applications of the proposed dual-signal bioassay in living cells. As shown in Fig. 5B, HeLa, MCF-7 and HepG2 cell lysates produced obvious ΔI_{EC} and $|\Delta I_{PEC}|$ signal responses, while no significant signal was detected toward lysis buffer. To further confirm that the observed signal responses were exclusively generated by active UDG activity in the cell lysates rather than any other component in the lysates, the uracil-DNA glycosylase inhibitor (UGI) was added into the cell lysate to inhibit the UDG activity, which could combine closely with UDG to form a physiologically irreversible complex. As expected, with the addition of UGI, the ΔI_{EC} and $|\Delta I_{PEC}|$ signal responses significantly decayed. In addition, selecting the cell lysate system containing UGI as the blank control, the actual ΔI_{EC} and $|\Delta I_{PEC}|$ signal contribution of UDG could be obtained by subtracting the ΔI_{EC} and $|\Delta I_{PEC}|$ of the blank control from that of the cell lysates sensing system. Bring signal value into the corresponding linear function $|\Delta I_{PEC}| = 26.28 + 5.87\ lgC_{UDG}$ (U/mL) and $\Delta I_{EC} = 17.64 + 3.97\ lgC_{UDG}$, the UDG activity could be calculated. For PEC (EC) strategy, the UDG activities were obtained as 2.91×10^{-2} (2.78×10^{-2}), 4.21×10^{-2} (3.98×10^{-2}) and 2.5s0 $\times 10^{-2}$ (2.3×10^{-2}) U/mL toward HeLa, HepG2 and MCF-7 cancer cells, respectively. Furthermore, a BCA protein assay kit was used to measure the total amount of the protein in the HeLa, HepG2 and MCF-7 cell lysates, and the total amount of the protein concentration was 0.10 mg/mL, 0.12 mg/mL and 0.10 mg/mL, respectively. Thus, the UDG activity in the HeLa, MCF-7 and HepG2 cell lysate were determined as 0.28 U/mg, 0.34 U/mg and 0.24 U/mg (U UDG per mg total protein), which was close to the those reported literature [Du et al., 2018; Tao et al., 2015; Wu et al., 2016]. These results demonstrated that the developed dual-signal bioassay has a great potentiality to detect UDG activity in living cells.

4. Conclusion

In summary, an efficient dual-signal bioassay for sensitive and accurate analysis of UDG activity was proposed by integrating PEC with EC strategies in one probe electrode. Both the “signal-off” trend for PEC signal and the “signal-on” trend for EC signal were simultaneously triggered by the target UDG induced cleavage of sDNA on the Au/TiO_2 hybrid matrix. For PEC strategy, the cleavage of sDNA induced the disappearance in sensitization effect of PEC labels of AIS QDs and caused the generation of obvious steric hindrance by the long double-

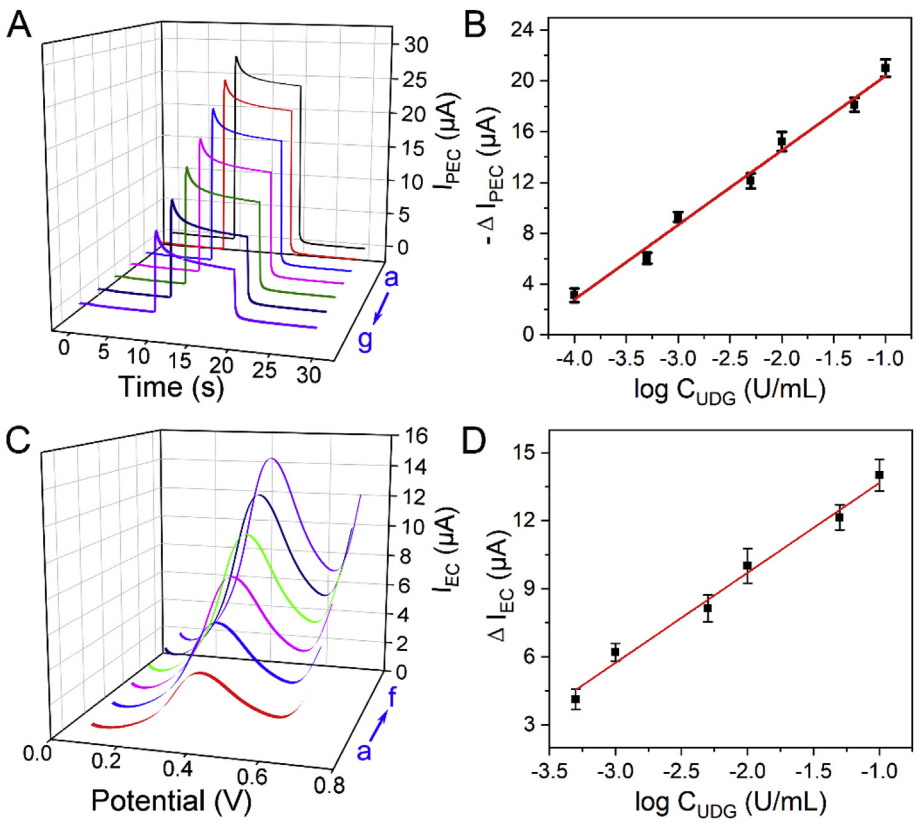

Fig. 4. (A) PEC signals of the dual-signal bioassay with increased concentration of UDG (curves a to g: 1.0×10^{-4}, 5.0×10^{-4}, 1.0×10^{-3}, 5.0×10^{-3}, 1.0×10^{-2}, 5.0×10^{-2} and 0.1 U/mL), and (B) corresponding calibration curve between $-\Delta I_{PEC}$ and logarithm of UDG concentration. (C) EC signals of the dual-signal bioassay with increased concentration of UDG (curves a to f: 5.0×10^{-4}, 1.0×10^{-3}, 5.0×10^{-3}, 1.0×10^{-2}, 5.0×10^{-2}, and 0.1 U/mL), and (D) corresponding calibration curve between ΔI_{EC} and logarithm of UDG concentration. The error bars display the standard deviation of five parallel measurements.

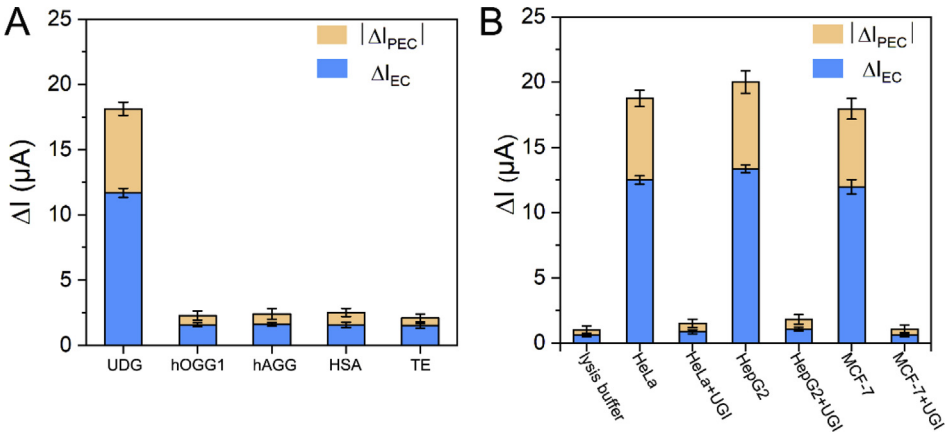

Fig. 5. (A) ΔI_{EC} and $|\Delta I_{PEC}|$ signals of the dual-signal bioassay toward UDG (0.05 U/mL), hOGG1 (0.1 U/mL), hAGG (0.1 U/mL), HSA (1 mg/mL), and TE (0.1 U/mL). (B) ΔI_{EC} and $|\Delta I_{PEC}|$ signals of the dual-signal bioassay toward lysis buffer, HeLa, HepG2 and MCF-7 cell lysates in the absence or presence of UGI. The error bars show the standard deviation of five parallel measurements.

stranded DNA via the HCR process. For EC strategy, the cleavage of sDNA guided the aDNA assembly and then triggered the HCR process, resulting in the introduction of abundant EC labels of ferrocene molecules. The elaborated dual-signal bioassay exhibited the obvious merits of low detection limit, broad linear range, excellent specificity and well stability, and its practical application for accurate and reliable detection of UDG activity in different living cells was achieved. The further study on more advanced dual-signal bioassay for other DNA repair-related enzymes in the real samples is underway.

Declaration of interest statement

We herein declare that we have no financial and personal relationships with other people or organizations that can inappropriately influence our work, and there is no professional or other personal interest of any nature or kind in any product, service and/or company that could be construed as influencing the position presented in, or the review of, the manuscript entitled.

CRediT authorship contribution statement

Yanwei Lu: Data curation, Formal analysis, Investigation, Methodology. **Huan Zhao:** Data curation, Formal analysis, Investigation, Methodology. **Gao-Chao Fan:** Conceptualization, Supervision, Validation, Visualization, Writing - original draft. **Xiliang Luo:** Writing - review & editing.

Acknowledgments

This work is supported by the National Natural Science Foundation of China (21603099), the Taishan Scholar Program of Shandong Province of China (ts20110829), and the Project Fund for Shangdong Key R&D Program (2019GSF108175).

Appendix A. Supplementary data

Supplementary data to this article can be found online at https://

doi.org/10.1016/j.bios.2019.111569.

References

Ameta, R., Benjamin, S., Sharma, S., Trivedi, M., 2015. Sol. Energy Convers. Storage Photochem. Modes 414, 85–113.
Boorstein, R.J., Cummings, A., Marenstein, D.R., Chan, M.K., Ma, Y., Neubert, T.A., Brown, S.M., Teebor, G.W., 2001. J. Biol. Chem. 276, 41991–41997.
Burrell, R.A., McGranahan, N., Bartek, J., Swanton, C., 2013. Nature 501, 338–345.
David, S.S., Williams, S.D., 2002. Chem. Rev. 98, 1221–1262.
Dong, J., Lian, J., Jin, Y., Li, B., 2017. Anal. Methods 9, 276–281.
Du, W., Li, J., Xiao, F., Yu, R., Jiang, J., 2017. Anal. Chim. Acta 991, 127–132.
Du, Y.C., Cui, Y.X., Li, X.Y., Sun, G.Y., Zhang, Y.P., Tang, A.N., Kim, K., Kong, D.M., 2018. Anal. Chem. 90, 8629–8634.
Duncan, B.K., Miller, J.H., 1980. Nature 287, 560–561.
Fan, G.C., Zhao, M., Zhu, H., Shi, J.J., Zhang, J.R., Zhu, J.J., 2016a. J. Phys. Chem. C 120, 15657–15665.
Fan, G.C., Zhu, H., Du, D., Zhang, J.R., Zhu, J.J., Lin, Y., 2016b. Anal. Chem. 88, 3392–3399.
Forment, J.V., Kaidi, A., Jackson, S.P., 2012. Nat. Rev. Cancer 12, 663.
Guan, P., Bai, H., Li, C., Ge, Y., Xu, D., Chen, B., Xia, T., Fan, W., Shi, W., 2018. Adv. Mater. Interfaces 5, 2–9.
Gupta, P.K., Sirover, M.A., 2006. Proc. Natl. Acad. Sci. 81, 757–761.
Hegde, M.L., Hazra, T.K., Mitra, S., 2008. Cell Res. 18, 27.
Hoeijmakers, J.H.J., 2001. Nature 411, 366–374.
Hu, Q., Han, D., Gan, S., Bao, Y., Niu, L., 2018. Anal. Chem. 90, 12207–12213.
Imai, K., Slupphaug, G., Lee, W.I., Revy, P., Nonoyama, S., Catalan, N., Yel, L., Forveille, M., Kavli, B., Krokan, H.E., Ochs, H.D., Fischer, A., Durandy, A., 2003. Nat. Immunol. 4, 1023–1028.
Jiang, X.-Y., Chen, H.-Y., Yu, X.-D., Xu, J.-J., Mei, L.-P., Zhao, W.-W., 2018. Anal. Chem. 90, 2749–2755.
Jiao, F., Qian, P., Qin, Y., Xia, Y., Deng, C., Nie, Z., 2016. Talanta 147, 98–102.
Ledoux, S., Wilson, G., 2004. FEBS Lett. 476, 273–284.
Lee, C.Y., Park, K.S., Park, H.G., 2015. Chem. Commun. 51, 13744–13747.
Leung, K.H., He, H.Z., Ma, V.P.Y., Zhong, H.J., Chan, D.S.H., Zhou, J., Mergny, J.L., Leung, C.H., Ma, D.L., 2013. Chem. Commun. 49, 5630–5632.
Li, K., Chai, B., Peng, T., Mao, J., Zan, L., 2013. ACS Catal. 3, 170–177.
Li, M., Xiong, C., Zheng, Y., Liang, W., Yuan, R., Chai, Y., 2018. Anal. Chem. 90, 8211–8216.
Liu, X., Chen, M., Hou, T., Wang, X., Liu, S., Li, F., 2014. Biosens. Bioelectron. 54, 598–602.
Liu, X., Chen, M., Hou, T., Wang, X., Liu, S., Li, F., 2013. Electrochim. Acta 113, 514–518.
Lord, C.J., Ashworth, A., 2012. Nature 481, 287–294.
Mars, A., Hamami, M., Bechnak, L., Patra, D., Raouafi, N., 2018. Anal. Chim. Acta 1036, 141–146.
Maynard, S., Schurman, S.H., Harboe, C., de Souza-Pinto, N.C., Bohr, V.A., 2009. Carcinogenesis 30, 2–10.
Nie, H., Wang, W., Li, W., Nie, Z., Yao, S., 2015. Analyst 140, 2771–2777.
Qiu, Z., Shu, J., Liu, J., Tang, D., 2019. Anal. Chem. 91, 1260–1268.
Regulacio, M.D., Win, K.Y., Lo, S.L., Zhang, S.Y., Zhang, X., Wang, S., Han, M.Y., Zheng, Y., 2013. Nanoscale 5, 2322–2327.
Saidur, M.R., Aziz, A.R.A., Basirun, W.J., 2017. Biosens. Bioelectron. 90, 125–139.
Savva, R., Mc Auley-Hecht, K., Brown, T., 1995. Nature 373, 487–493.
Song, Y., Luo, Y., Zhu, C., Li, H., Du, D., Lin, Y., 2016. Biosens. Bioelectron. 76, 195–212.
Sousa, M.M.L., Krokan, H.E., Slupphaug, G., 2007. Mol. Asp. Med. 28, 276–306.
Sud'ina, A.E., Volkov, E.M., Oretskaya, T.S., Degtyarev, S.K., Gonchar, D.A., Kubareva, E.A., 2000. Russ. J. Bioorganic Chem. 26, 398–402.
Tao, J., Song, P., Sato, Y., Nishizawa, S., Teramae, N., Tong, A., Xiang, Y., 2015. Chem. Commun. 51, 929–932.
Wang, G.L., Shu, J.X., Dong, Y.M., Wu, X.M., Li, Z.J., 2015. Biosens. Bioelectron. 66, 283–289.
Wang, L.J., Ren, M., Zhang, Q., Tang, B., Zhang, C.Y., 2017. Anal. Chem. 89, 4488–4494.
Werner, R.M., Stivers, J.T., 2000. Biochemistry 39, 14054–14064.
Wu, Y., Wang, L., Zhu, J., Jiang, W., 2015. Biosens. Bioelectron. 68, 654–659.
Wu, Y., Yan, P., Xu, X., Jiang, W., 2016. Analyst 141, 1789–1795.
Xiang, J., Pi, X., Chen, X., Xiang, L., Yang, M., Ren, H., Shen, X., Qi, N., Deng, C., 2017. Biosens. Bioelectron. 96, 268–274.
Xu, X., Hou, R., Gao, P., Miao, M., Lou, X., Liu, B., Xia, F., 2016. Anal. Chem. 88, 2386–2391.
Zarazúa, I., De la Rosa, E., López-Luke, T., Reyes, J., Ruiz, S., 2010. Next gener. Photonic cell technol. Sol. Energy Convers. 7772, 777217.